J Mater Sci (2010) 45:5228–5236
DOI 10.1007/s10853-010-4563-8

Cathodoluminescence properties of SiO_2:$Pr^{3+}$and ZnO·SiO_2:Pr^{3+} phosphor nanopowders

G. H. Mhlongo · O. M. Ntwaeaborwa · M. S. Dhlamini · H. C. Swart · K. T. Hillie

Received: 28 January 2010 / Accepted: 26 April 2010 / Published online: 8 May 2010
© Springer Science+Business Media, LLC 2010

Abstract The successful incorporation of ZnO nanoparticles in Pr^{3+}-doped SiO_2 using a sol–gel process is reported. SiO_2:Pr^{3+} gels, with or without ZnO nanoparticles, were dried at room temperature and annealed at 600 °C. On the basis of the X-ray Diffraction (XRD) results, the SiO_2 was amorphous regardless of the incorporation of Pr^{3+} and nanocrystalline ZnO or annealing at 600 °C. The particles were mostly spherical and agglomerated as confirmed by Field Emission Scanning Electron Microscopy. Thermogravimetric analysis of dried gels performed in an N_2 atmosphere indicated that stable phases were formed at ≥900 °C. Absorption bands ascribed to $^3H_4$-$^3P_{(J\,=\,0,1,2)}$, $^1I_6$ and $^1D_2$ in the UV–VIS region were observed from SiO_2:Pr^{3+} colloids. The red cathodoluminescent (CL) emission corresponding to the $^3P_0 \rightarrow {}^3H_6$ transition of Pr^{3+} was observed at 614 nm from dried and annealed SiO_2:Pr^{3+} powder samples. This emission was increased considerably when ZnO nanoparticles were incorporated. The CL intensity was measured at an accelerating voltage of 1-5 keV and a fixed beam current of 8.5 μA. The effects of accelerating voltage on the CL intensity and the CL degradation of SiO_2:Pr^{3+} and ZnO·SiO_2:Pr^{3+} were also investigated using Auger electron spectroscopy coupled with an Ocean Optics S2000 spectrometer.

G. H. Mhlongo · M. S. Dhlamini · K. T. Hillie (✉)
National Centre for Nano-structured Materials, CSIR, P.O. Box 395, Pretoria 0001, South Africa
e-mail: thillie@csir.co.za

G. H. Mhlongo
e-mail: GMhlongo@csir.co.za

G. H. Mhlongo · O. M. Ntwaeaborwa · H. C. Swart · K. T. Hillie
Department of Physics, University of the Free State, Bloemfontein 9300, South Africa

O. M. Ntwaeaborwa
e-mail: ntwaeab@ufs.ac.za

H. C. Swart
e-mail: swarthc@ufs.ac.za

Introduction

Research interest in the study of trivalent praseodymium (Pr^{3+}) ions incorporated in different solid hosts has lately grown tremendously. The research work that has been done on Pr^{3+} has provided an excellent understanding of the main features of this ion. Depending on the host matrix, Pr^{3+} can emit efficiently in the blue, green, orange, red and near infrared (NIR) regions [1, 2]. Its energy level diagram consists of several metastable multiplets, namely $^3P_{0,1,2}$, $^1D_2$ and $^1G_4$ [3]. Its energy level structure permits various linear and non linear effects, like UV tunable luminescence from low-lying 4f5d levels, visible emissions from either $^3P_0$ or $^1D_2$ states leading to blue-greenish, or red emissions, respectively. Infrared to blue or red to blue photon conversion due to anti-Stokes processes is also possible [4]. Pr^{3+} emissions in the UV–VIS region can be used for laser action while those in the IR region can be used for optical amplification at 1.3 μm [5]. Semiconductor materials emitting light in the 1.3 or 1.55 μm regimes are of substantial importance for applications in telecommunications.

The Pr^{3+} ion has been studied in numerous hosts such as crystals [4–6], and glasses [1, 2, 7–16]. The emission from Pr^{3+} ion strongly depends on the host lattice [3]. It has been widely reported that when this ion is incorporated in oxide-based lattices, it exhibits an intense red emission from $^1D_2$ level ($^1D_2 \rightarrow {}^3H_4$ transition) connected with partial and, in some cases, complete quenching of the greenish-blue emission from $^3P_0$ level, depending on the nature of the host lattice and its constituents [3, 4]. For example, Diallo et al. [17]

reported a single prominent red emission at 613 nm attributed to the $^1D_2 \rightarrow {}^3H_4$ transition when Pr^{3+} was doped in a $CaTiO_3$ crystal. Annapurna et al. [9], on the other hand, observed the intense red luminescence from both the $^1D_2 \rightarrow {}^3H_4$ and $^3P_0 \rightarrow {}^3H_6$ transitions when Pr^{3+} was incorporated in different types of glasses such as SiO_2, Al_2O_3, BaF_2 and GdF_3. Numerous studies on Pr^{3+}-doped silica glasses have also been conducted to evaluate the optical absorption and emission properties of Pr^{3+} [8, 14–16].

Field emission displays (FEDs) technology operates at low voltages (300 V to 10 kV) and much high current densities ($\sim$100 μA/cm^2) compared to Cathode Ray Tubes (CRTs) which operate at 25–30 kV and low current densities [18]. Phosphors with high luminous efficiency and thermal stability are regarded as the best candidates for application in this technology. One of the problems that affect the performance of FEDs and limits their commercialization is degradation of the phosphors at high current density under prolonged electron bombardment. In particular, sulphide-based phosphors which are widely used in display technology have been found to degrade drastically under prolonged electron-beam bombardment [19]. In addition, they degrade by releasing some volatile compounds which are detrimental to the emitter tips of the FEDs. On the other hand, oxide-based phosphors have been reported to be more chemical and thermodynamically stable under high current densities, high-vacuum pressures as well as at elevated temperatures [20]. As a result, research interest in the development and investigation of oxide phosphors, as possible candidates to replace sulphide-based phosphors in low voltage FEDs, has increased considerably lately. For example, Ntwaeaborwa et al. have investigated the CL degradation of SiO_2:Ce^{3+}, Tb^{3+} [21] and Y_2O_3:Eu^{3+} [22] in the presence of O_2. In the case of SiO_2:Ce^{3+}, Tb^{3+} they attributed the CL degradation to the non luminescent SiO_x ($x < 2$) formed as a result of desorption of O from the surface. Y_2O_3:Eu^{3+} was found to be chemically stable after prolonged bombardment by 2 keV electrons and the CL degradation was therefore attributed to non-radiative de-excitation mechanism rather than the formation of a dead layer on the surface. In this work, the CL properties of SiO_2, SiO_2:Pr^{3+} and ZnO·SiO_2:Pr^{3+} phosphor powders and their CL degradation mechanisms are discussed. These phosphors are evaluated for possible applications in low voltage FED.

Experimental procedure

Sample preparation by sol–gel method

ZnO nanocrystals

The preparation of colloidal solutions of ZnO nanoparticles in alcohols has been investigated in the past [23, 24]. To obtain a sol of ZnO nanocrystals, 0.459 g $Zn(CH_3COO)_2{\cdot}2H_2O$ was dissolved in 30 mL of boiling absolute ethanol and stirred to form a transparent solution and cooled in ice water. A solution of 0.2 g of NaOH dissolved in 10 mL of absolute ethanol at room temperature in an ultrasonic bath was cooled in ice water and added dropwisely to the ethanol suspension of Zn^{2+} under vigorous stirring. The resulting clear sol was kept at room temperature for 24 h followed by centrifuging and washing repeatedly with heptane to remove unwanted Na^+ and CH_3COO^- ions. The resulting ZnO precipitate was re-dispersed in ethanol or dried at 90 °C for 2 h.

SiO_2:Pr^{3+} and ZnO·SiO_2:Pr^{3+}

Pr^{3+}-doped SiO_2 samples were prepared using a sol–gel process from a starting mixture of tetraethyl orthosilicate ($Si(OC_2H_5)_4$), or TEOS, de-ionized water, ethanol, nitric acid (HNO_3) as a catalyst), and $Pr(NO)_3{\cdot}6H_2O$. The mixture of 0.05 mol of TEOS, 0.1 mol of H_2O, 0.1 mol of ethanol and 0.145 mol of dilute nitric acid was stirred at room temperature for 1 h to get a clear solution followed by slow addition of 1 mol% of $Pr(NO)_3{\cdot}6H_2O$ dissolved in 5 mL of ethanol and stirred for 30 min. The obtained SiO_2:Pr^{3+} (1 mol%) was divided into two, the first part was transferred into a petri dish for drying and the second part was combined with the ethanol suspension of 1 mol% ZnO nanoparticles. The second solution was stirred vigorous for 1 h at room temperature. The gels were dried at room temperature for 8 days, ground using a mortar and pestle and then heat treated at 600 °C for 2 h in ambient air.

Characterization

ZnO, SiO_2, SiO_2:Pr^{3+} and ZnO SiO_2:Pr^{3+} nanopowders were characterized by X-ray diffraction (Phillips Xpert) using a Cu Kα ($\lambda = 1.5405$ Å) radiation. The crystallite size of the ZnO nanoparticles was estimated from the Debye–Scherrer equation. Thermogravimetric Analysis (TGA) of the dried gels was carried out under a nitrogen atmosphere at a heating rate of 10 °C/min at the temperature range of 50–950 °C using a TGA Q500 (TA instruments). CL spectra in the UV–IR range were collected using an Ocean Optics S2000 spectrometer attached to an ultra high vacuum (UHV) chamber of a PHI 549 Auger electron spectrometer. Optical absorption spectra were recorded from colloids of ZnO, Pr^{3+}-doped and un-doped SiO_2 using a Perkin Elmer Lamda 750S UV–VIS spectrometer in the wavelength range of 350–700 nm. The particle morphology was analyzed using a JEOL JSM-7500F, Field Emission Scanning Electron Microscope (FESEM).

Results and discussions

Sample structure (XRD)

Figure 1 shows the XRD patterns of the ZnO nanoparticles and the standard ZnO microparticles powders corresponding to the ZnO hexagonal structure. The broadening of the ZnO diffraction peaks is attributed to the smaller particle sizes. The average crystallite size of the ZnO nanoparticles estimated from Scherrer's equation was ~4 nm. With or without the Pr^{3+} and the ZnO nanoparticles, SiO_2 was amorphous even after annealing at 600 °C for 2 h (see Fig. 2). This was probably due to the relatively low concentration of Pr^{3+} and the ZnO nanoparticles and/or high amorphous scattering background from the SiO_2 matrix

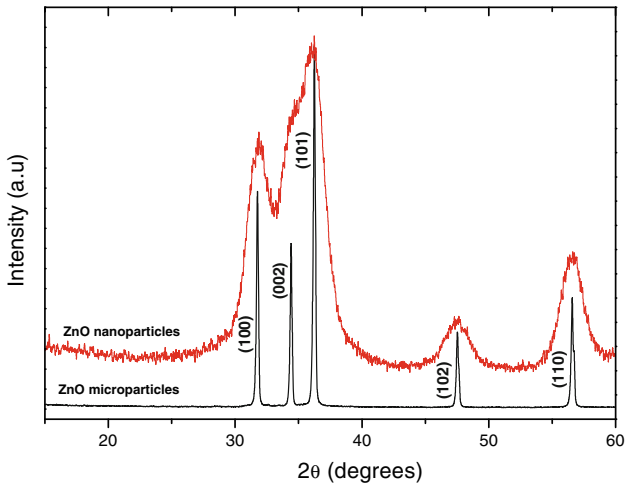

Fig. 1 XRD patterns of the ZnO nanoparticles and microparticles

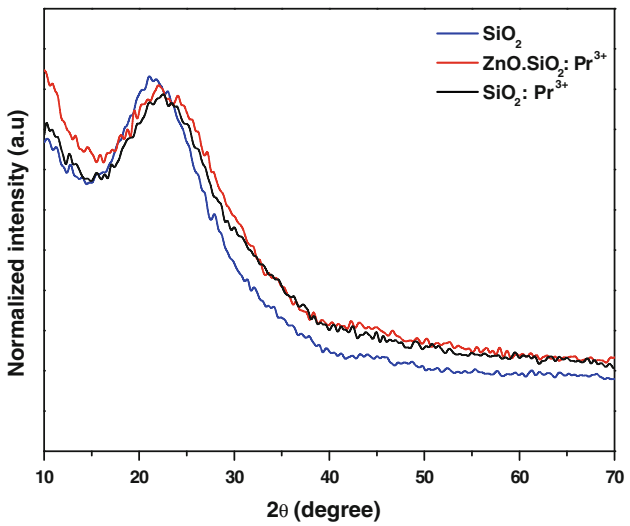

Fig. 2 XRD patterns of SiO_2, SiO_2:Pr^{3+} and ZnO·SiO_2:Pr^{3+} nanopowders calcined at 600 °C for 2 h

[25]. The presence of the Pr^{3+} and ZnO nanoparticles in the phosphor powders (not shown) was confirmed by Electron Dispersive Spectroscopy (EDS).

Sample morphology (FESEM)

The FESEM images in Fig. 3(a–c) illustrate the morphologies of the SiO_2, SiO_2:Pr^{3+}, and ZnO·SiO_2:Pr^{3+} nanopowders calcined at 600 °C for 2 h. The images revealed that the particles were agglomerated and mostly spherical in shape with an average particle size in the range of ~20–30 nm in diameter.

Thermal analysis, TGA

The TGA curves of SiO_2, SiO_2:Pr^{3+} and ZnO·SiO_2:Pr^{3+} are presented in Fig. 4. The first weight loss was observed at temperatures between 50 and 130 °C and it can be ascribed to loss of physically adsorbed water and ethanol [26]. The second weight loss at 250–600 °C corresponds to relaxation of silica network and oxidation of residual organics. The weight loss was shown to decrease as the temperature exceeded 600 °C until stable phases formed at ≥900 °C. The total weight loss for SiO_2, SiO_2:Pr^{3+}, and ZnO·SiO_2:Pr^{3+} was ~19%, ~25% and ~22%, respectively. It can be seen that the rate of weight loss was faster in Pr^{3+} and/or ZnO-doped SiO_2 samples. This could be due to enlargement in the pore volume and surface area of gels with introduction of 1 mol% Pr^{3+} and 1 mol% of ZnO nanoparticles in the SiO_2 matrix. Biswas et al. [26] reported an increase in total weight loss with increasing Pr^{3+} content (i.e., 22%, 29% and 32% for SiO_2, SiO_2:Pr^{3+} (5 wt%) and SiO_2:Pr^{3+} (10 wt%), respectively). Naturally, the gels are microporous and consist of large number of internal silanol groups. When the gel is heat treated, the pores collapse gradually as temperature increases and convert to pore-free materials similar to silica gels [26]. As a result, the hydrogen-bonded silanol groups release water to produce Si–O–Si bonds, and then the steam gives rise to foaming of densified gels which occurs at elevated temperatures as reported by Biswas et al. [26].

Optical absorption and emission properties (UV–VIS and CL)

The optical absorption spectrum of Pr^{3+}-doped and un-doped SiO_2 are presented in Fig. 5. The Pr^{3+}-doped SiO_2 revealed four bands in the UV–VIS region all originating from ground state $^3H_4$ to several excited states of the Pr^{3+} ions. These absorption bands are assigned to $^3H_4$–$^3P_{(J\,=\,0,1,2)}$, $^1I_6$ and $^1D_2$ $4f^2$ intraconfigurational electric dipole transitions of the Pr^{3+}. These compare very well with the results reported by several researchers [1, 2, 8, 14–16].

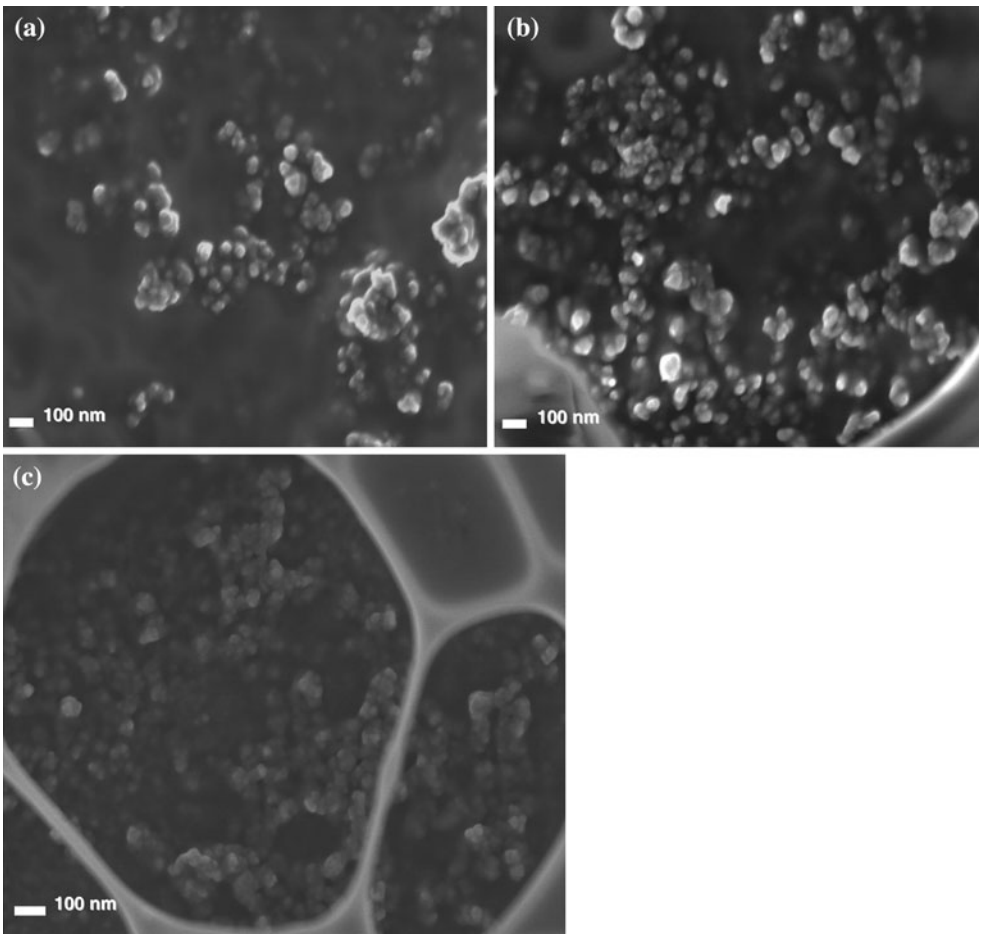

Fig. 3 HRSEM images of (**a**) SiO_2-, (**b**) Pr^{3+}-doped SiO_2 and (**c**) $ZnO{\cdot}SiO_2{:}Pr^{3+}$ nanophosphor powders

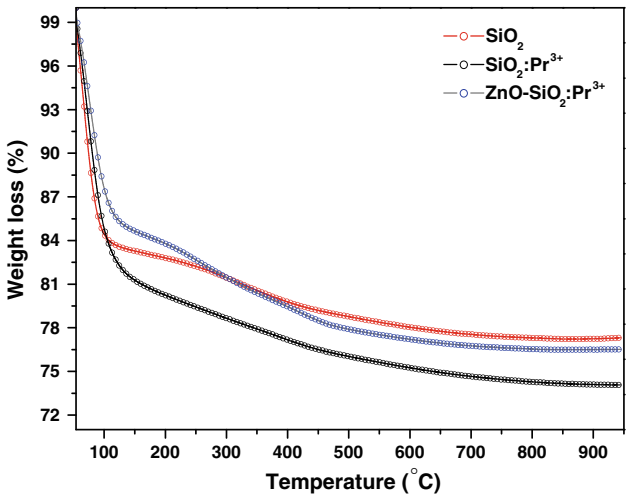

Fig. 4 TGA curves of un-doped SiO_2, $SiO_2{:}Pr^{3+}$ and $ZnO{\cdot}SiO_2{:}Pr^{3+}$ phosphor gels. The samples were heated from 50 to 950 °C in N_2 atmosphere at a heating rate of 10 °C/min

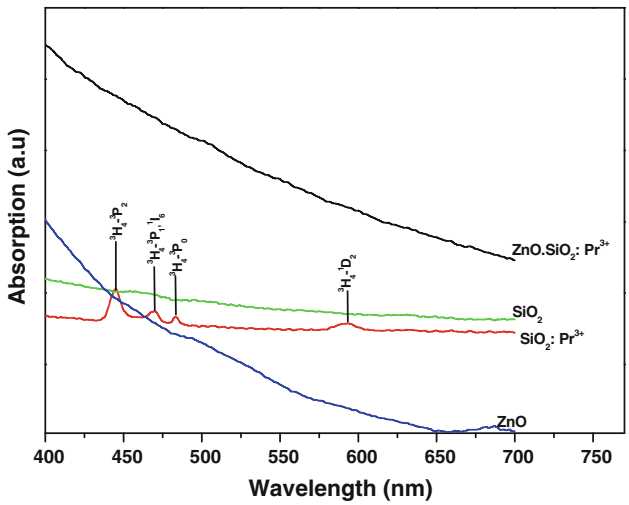

Fig. 5 UV–VIS absorption spectra of SiO_2, ZnO, $SiO_2{:}Pr^{3+}$, and $ZnO{\cdot}SiO_2{:}Pr^{3+}$

CL spectra of the SiO_2, $SiO_2{:}Pr^{3+}$ and $ZnO{\cdot}SiO_2{:}Pr^{3+}$ nanophosphor powders excited by 2 keV electrons, at 20 μA current density in a high-vacuum chamber at a base pressure of $\sim 1.6 \times 10^{-8}$ Torr are shown in Fig. 6. The CL spectrum of SiO_2 showed the emission peak at 445 nm. This peak can be either due to structural defects in the SiO_2

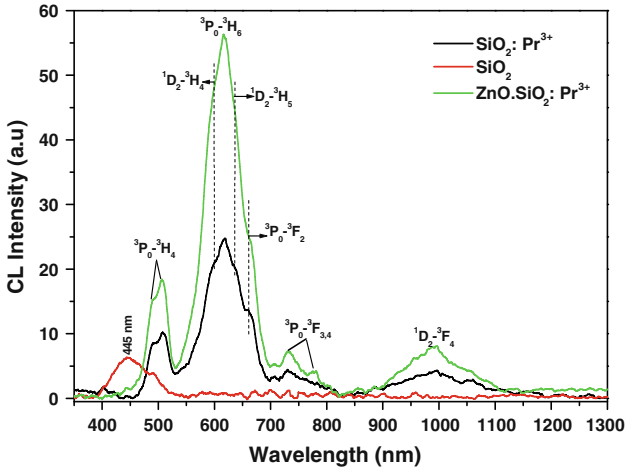

Fig. 6 CL spectra of un-doped SiO_2, SiO_2:Pr^{3+} and $ZnO{\cdot}SiO_2$:Pr^{3+} irradiated with 2 kV, 20 μA beam of electrons in a high-vacuum chamber containing 1.6×10^{-8} Torr

network or charge transfer between O and Si atoms [27]. The characteristic emission peaks with maximum emission at 614 nm, can be associated with transitions in Pr^{3+}, were observed from both SiO_2:Pr^{3+} and $ZnO{\cdot}SiO_2$:Pr^{3+}samples. This emission can be assigned to the transitions originating from the $^3P_0$ and $^1D_2$ energy levels to the $^3H_{(J=6,5,4)}$ and $^3F_{(J=2,3,4)}$ energy levels all localized in the $4f^2$ intraconfiguration of the Pr^{3+} ions. The first two peaks located at 488 and 510 nm are associated with the $^3P_0 \rightarrow {}^3H_4$ transition. Isasi-Marin et al. [28] reported three stark components from this transition when Pr^{3+} is doped in ZrO_2. This is followed by a broad emission peak with a dominant emission at 614 nm which is assigned to the $^3P_0 \rightarrow {}^3H_6$ transition.

The shoulders at 590, 635 and 661 nm correspond to $^1D_2 \rightarrow {}^3H_4$, $^1D_2 \rightarrow {}^3H_5$, and $^3P_0 \rightarrow {}^3F_2$ transitions, respectively. The assignment of these peaks compares well with the fluorescence spectra reported by Annapurna et al. [9] and Rai et al. [2] for Pr^{3+}-doped tellorite glasses. The overlay of the two transitions ($^3P_0 \rightarrow {}^3H_6$ and $^1D_2 \rightarrow {}^3H_4$) in Pr^{3+}-doped glasses was also observed by Annapurna et al. [9]. In order to explain the overlay of both emission transitions, Annapurna et al. [9] conducted the decay lifetime measurements of the excited states of the $^3P_0$ and $^1D_2$ levels and found that the $^3P_0$ excited state decayed faster than the $^1D_2$. This suggests that the luminescence is from the $^1D_2$ level. According to the observation of Lakshminarayana et al. [1], the $^3P_0$ excited state decayed slower than the $^1D_2$. The reason for such differences may be that the decay time measurements of the rare earths excited states differ from host to host since they strongly depend on the host lattice's phonon energies.

Lakshminarayana et al. [1] ascribed the absence of the luminescence from $^1D_2$ to the large energy gap between the $^3P_0$ and $^1D_2$ ($\sim 3858.5\ cm^{-1}$) resulting in a very small multiphonon non-radiative relaxation from $^3P_0$ to $^1D_2$. Such decay lifetime measurements were not conducted in the present study. The last peak in the NIR region centred at 995 nm is assigned to the $^1D_2 \rightarrow {}^3F_4$ transition. However, the peak position is different from the observation of Biswas et al. [26].

The well-known defects emission from ZnO nanoparticles at 530–560 nm was not observed from $ZnO{\cdot}SiO_2$:Pr^{3+} emission spectrum. The main emission peak from Pr^{3+} remained stable at 614 nm from both SiO_2:Pr^{3+} and $ZnO{\cdot}SiO_2$:Pr^{3+} samples. This confirms that incorporation of the ZnO nanoparticles did not change the radiative process of Pr^{3+} and this further suggest that the ZnO nanoparticles were well dispersed in the SiO_2 matrix [25]. It can also be observed that the blue emission from the host SiO_2 was also suppressed. The increase in the CL intensity of the 614 nm peak as a result of incorporation of ZnO nanoparticles suggests that energy was transferred from the ZnO nanoparticles to Pr^{3+} ions.

The energy transfer phenomenon between donors and acceptors in phosphors has been long known. This mechanism involves two luminescent centres, a Donor and an Acceptor (A and D) separated by a distance R with a certain interaction (i.e., exchange or multipole–multipole interaction) [3]. For instance, in $ZnO{\cdot}SiO_2$:Pr^{3+} the energy transfer takes place from a broadband emitter which is ZnO nanoparticles to a narrow-line absorber Pr^{3+}. This kind of process is only possible for nearest neighbours in the host lattice as reported by Blasse and Grabmaier [3]. For energy transfer process to occur between the energy donor (ZnO) and acceptor (Pr^{3+}), the distance R between the two must be shorter than the critical distance R_c (the critical distance at which ZnO emission dominates over energy transfer). This therefore means that 1 mol% of ZnO nanoparticle embedded in SiO_2 with 1 mol% Pr^{3+} has sufficiently short distance for energy transfer to dominate. The corresponding energy levels showing possible radiative transitions localized within the Pr^{3+} ion and energy transfer mechanism from ZnO nanoparticles to Pr^{3+} are presented schematically in Fig. 7. The enhancement of CL intensity at 614 nm with ZnO incorporation due to energy transfer process could be due to the fact that the defects states in the ZnO bandgap are filled by bandgap absorption and relaxation to the defects states of ZnO. The energy is therefore transferred possibly by phonon-mediated processes to the $^3P_0$ state of the Pr^{3+} ion via photoemission from ZnO and complete photocapture by Pr^{3+}, hence the enhanced Pr^{3+} emission was observed [29].

CL spectra of SiO_2:Pr^{3+} nanophosphor powders irradiated at different accelerating beam voltages (1–5 kV) and 8.5 μA in a high-vacuum chamber with a base pressure of $\sim 1.6 \times 10^{-8}$ Torr are shown in Fig. 8. From this figure, it

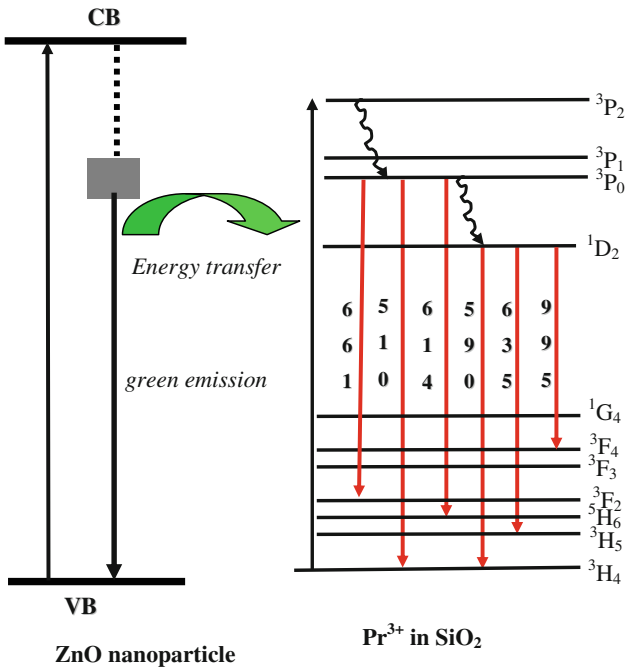

Fig. 7 Schematic representation of energy levels diagram depicting mechanism of energy transfer from ZnO nanoparticles and possible transitions in Pr^{3+}-doped in SiO_2

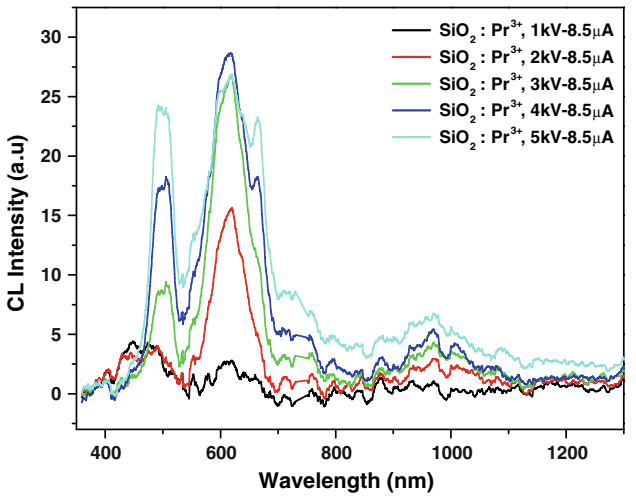

Fig. 8 CL spectra of SiO_2:Pr^{3+} irradiated with (1–5 kV), 8.5 μA beam of electrons in a high-vacuum chamber containing a base pressure of $\sim 1.6 \times 10^{-8}$ Torr

can be seen that with increased beam voltage from 1 to 5 kV, the CL intensity of the main emission peak at 614 nm first increased continuously up until it reached maximum at 4 kV, then decreased at 5 kV. This is clearly presented in Fig. 9 where the CL intensity is plotted against different electron-beam energies.

Figure 10 shows the CL spectra of ZnO·SiO_2:Pr^{3+} nanophosphor powders at an irradiation of different accelerating

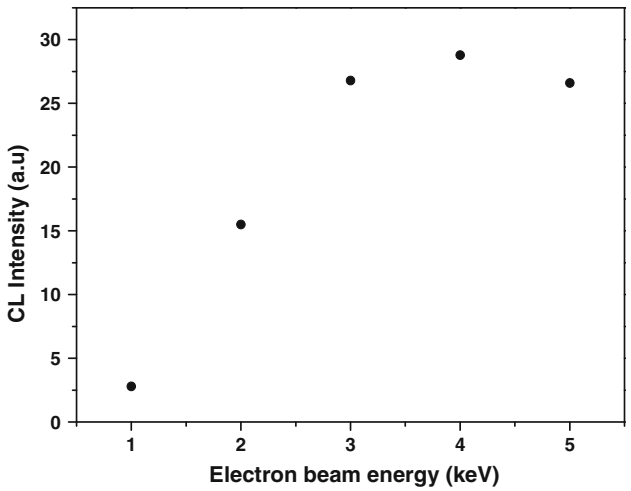

Fig. 9 CL intensity of SiO_2:Pr^{3+} 614 nm emission peak at different electron-beam voltages

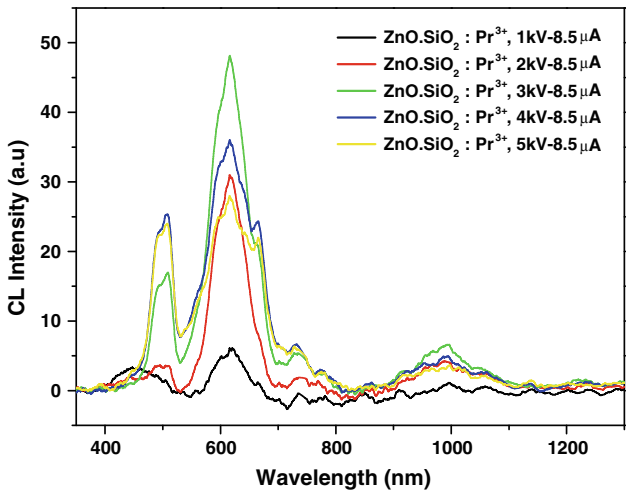

Fig. 10 CL spectra of ZnO·SiO_2:Pr^{3+} irradiated with 2 kV, 20 μA beam of electrons in a high-vacuum chamber containing a base pressure of $\sim 1.6 \times 10^{-8}$ Torr

beam voltages (1–5 kV) and 8.5 μA in a high-vacuum chamber with a base pressure of $\sim 1.6 \times 10^{-8}$ Torr. An increase in the CL intensity of the 614 nm peak from ZnO·SiO_2:Pr^{3+} with increasing beam voltage from 1 to 3 kV and its decrease as the voltage was further increased to 4 and 5 kV was observed (see Fig. 11). As the voltage was further increased up to 5 kV, the emission transitions from Pr^{3+} became more clearer, and their intensity was much higher than that observed from SiO_2:Pr^{3+}. This further confirms that energy was transferred from ZnO to Pr^{3+}.

The CL intensity plotted as a function of electron-beam energy follow the same trend as the electron impact ionization cross-section for an atom [30]. The intensity will first increase and then decrease with an increase in electron

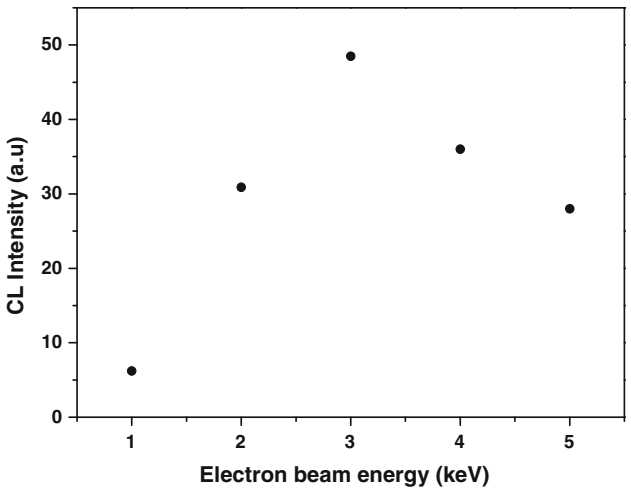

Fig. 11 CL intensity of $ZnO{\cdot}SiO_2{:}Pr^{3+}$ 614 nm emission peak at different electron-beam voltages

energy depending on the interaction of the electron with the atom. The decrease at higher energies are however more severe than expected, local heating beneath the beam and quenching due to charging are not excluded at higher energies [30].

The decrease in CL intensity of the main emission peak at 614 nm observed from both phosphors ($SiO_2{:}Pr^{3+}$ and $ZnO{\cdot}SiO_2{:}Pr^{3+}$) with increasing beam voltage can be tentatively explained by thermal quenching which occurs at high temperatures. When the beam voltage increases, the local heating by energetic electrons occurs, and thus temperature also increases which can cause thermal quenching. During thermal quenching, the thermal vibrations of atoms surrounding an activator ion transfers the energy away from the activator ion, as clearly explained by the configuration co-ordinate model [31], at high temperatures resulting in non-radiative recombination and a subsequent depletion of the excess energy as phonons in the host lattice.

CL degradation

The CL spectra from the $SiO_2{:}Pr^{3+}$ phosphor and the $ZnO{\cdot}SiO_2{:}Pr^{3+}$ phosphor before and after electron bombardment at an irradiation of 2 keV, 20 μA in an O_2 pressure of 1×10^{-7} Torr backfilled from a vacuum base pressure of 1.6×10^{-8} Torr are shown in Fig. 12(a) and (b), respectively. As shown in Fig. 12(a) and (b), the CL intensity of the 614 nm peak was degraded completely as a result of 2 keV electron bombardment.

The AES spectra of $SiO_2{:}Pr^{3+}$ and $ZnO{\cdot}SiO_2{:}Pr^{3+}$ phosphors before and after degradation (not shown) showed the Auger peaks of Si (80 eV), C (272 eV) and O (505 eV), respectively. It was noticed that with prolonged

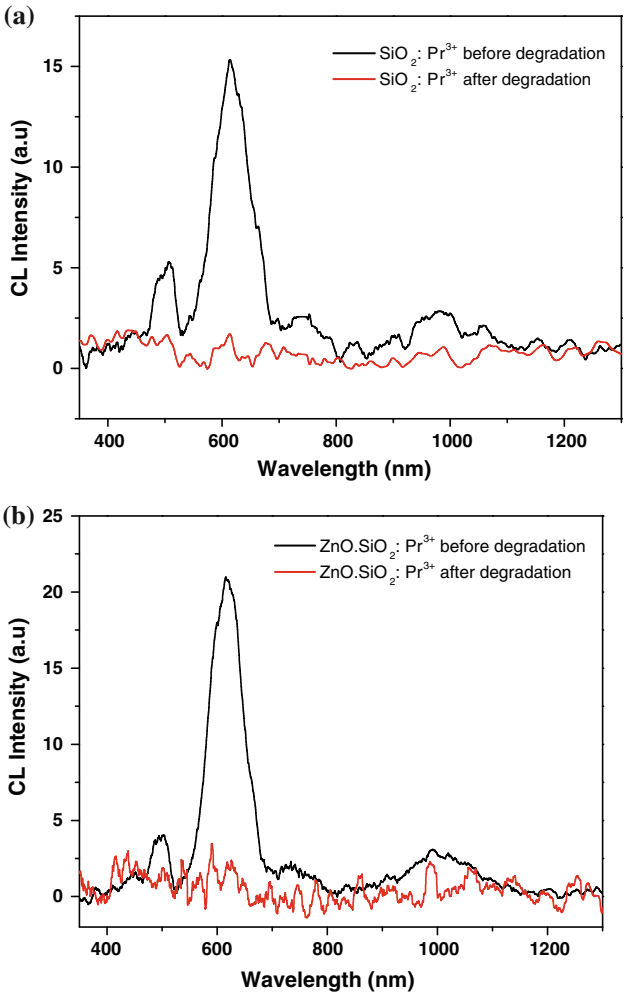

Fig. 12 CL spectra of (**a**) $SiO_2{:}Pr^{3+}$ and (**b**) $ZnO{\cdot}SiO_2{:}Pr^{3+}$ before and after electron bombardment by 2 kV, 20 μA in 1×10^{-7} Torr of O_2

electron bombardment of the SiO_2, the Auger peak intensity of Si and O decreased while that of adventitious C completely disappeared. The similar observation was reported by Ntwaeaborwa et al. [21]. Thomas et al. [32] reported the decrease in the Auger peak intensities of Si and O and the appearance of a new Auger peak located at ~92 eV associated with elemental Si. Ntwaeaborwa et al. [21] and Thomas et al. [32] reported that, the elemental Si in the SiO_2 compound can be shifted from higher energy (92 eV) to lower energy (75–80 eV), and this can be attributed to the change in the density of states and some relaxation effects involved.

Figure 13(a) and (b) shows the changes in the Auger peak-to-peak heights (APPH's) of Si, O and C from $SiO_2{:}Pr^{3+}$ and $ZnO{\cdot}SiO_2{:}Pr^{3+}$ phosphors, respectively, together with the CL intensity as a function of coulomb dose during 2 kV, 20 μA electron bombardment at 1×10^{-7} Torr of O_2 backfilled from a vacuum base pressure of 1.6×10^{-8} Torr. It was noticed that the

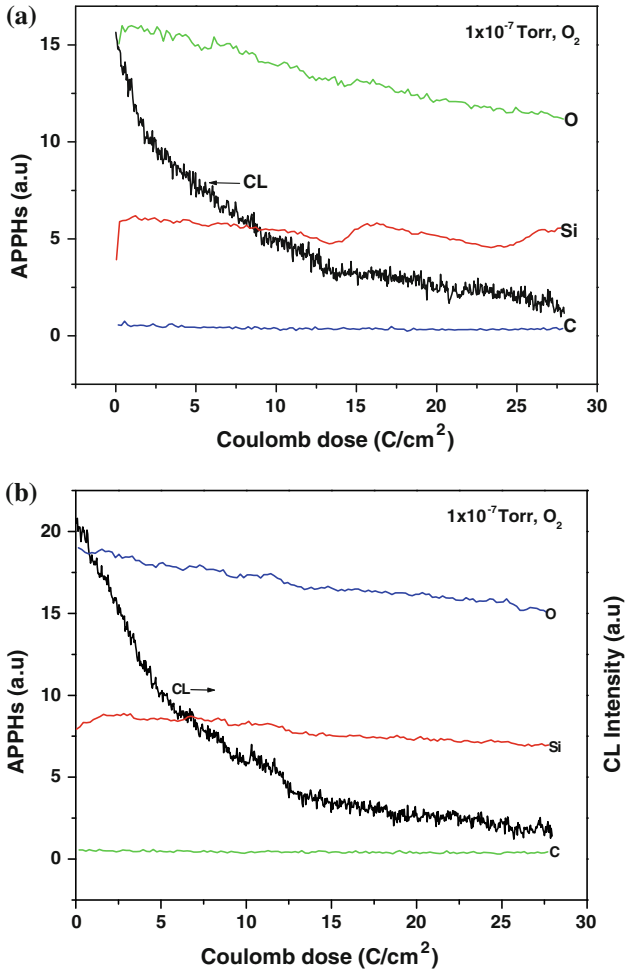

Fig. 13 AES peak-to-peak heights of (**a**) SiO_2:Pr^{3+} and (**b**) $ZnO{\cdot}SiO_2$:Pr^{3+} at 2 kV, 20 μA, in 1×10^{-7} Torr of O_2 as a function of electron dose

concentration of adventitious C on the surface was very small in both figures (a) and (b). The electron bombardment resulted in the decrease in O peak intensity while those of Si and C remained almost unchanged. The decrease in CL intensity as a result of electron bombardment was also observed from both SiO_2:Pr^{3+} and $ZnO{\cdot}SiO_2$:Pr^{3+} phosphors as indicated in figures (a) and (b). The correlation between the decrease of CL intensity and of the Auger peak intensity from O was recognized from this observation. Based on previous reports, this can be due to desorption of O from the surface following the electron-beam dissociation of SiO_2 [21].

Ntwaeaborwa et al. [21], Dhlamini et al. [33] attributed desorption of O_2 from the surface to electron stimulated surface chemical reactions (ESSCR). With prolonged electron bombardment, it is reported that the Si–O bonds are broken and free oxygen is released as ions following a reaction with dissociated species (e.g., C, H, or O) from vacuum ambient gasses (e.g., H_2O, O_2 and CO_2) [21, 33]. The ESSCR mechanism can also result in reduction of the radiative efficiency of the activators as it can cause incorporation of O iso-electronic traps in the near surface region. In the present results, we could not observe the new Auger peak associated with elemental Si at 92 eV in the AES spectra (not shown) after an electron of 27 C/cm^2 as documented by Thomas et al. and it could be that the desorption of oxygen resulted in the formation of an oxygen-deficient surface dead layer of SiO_x, where $x < 2$ consistent with the data reported in [21]. It is, therefore, reasonable to conclude that the SiO_x dead layer formed on the surface could be the main reason for degradation of the CL intensity of the SiO_2:Pr^{3+} and $ZnO{\cdot}SiO_2$:Pr^{3+} phosphors.

Conclusion

ZnO nanoparticles with an average crystallite size of ~4 nm, as estimated from Scherer equation, were successfully incorporated in Pr^{3+}-doped SiO_2 nanophosphor using a sol–gel method. It was shown that the enhanced red emission centred at 614 nm attributed to $^3P_0 \rightarrow {}^3H_6$ transition of Pr^{3+} was obtained from $ZnO{\cdot}SiO_2$:Pr^{3+}. The green emission from ZnO at ~530 nm was completely suppressed due to the non-radiative transfer of energy from ZnO to Pr^{3+}. The effect of the beam voltage in the CL intensity from both SiO_2:Pr^{3+} and $ZnO{\cdot}SiO_2$:Pr^{3+} was investigated. The degradation mechanism of SiO_2:Pr^{3+} and $ZnO{\cdot}SiO_2$:Pr^{3+} phosphor powders have been also discussed.

Acknowledgements The authors would like to thank Mart-Mari Biggs for assisting with CL measurements. This project is financially supported by the Department of Science and Technology of South Africa and the Council for Scientific and Industrial Research of South Africa.

References

1. Lakshminarayana G, Qiu J (2009) J Alloy Compd 476:470
2. Rai VK, Kumar K, Rai SB (2009) Optical Mater 29:873
3. Blasse G, Grabmaier BC (1994) Luminescent materials. Springer-Verlag, Berlin
4. Pinel E, Boutnaud P, Mahiou R (2004) J Alloy Compd 374:165
5. Balda R, Voda M, Al-Saleh M, Fernandez J (2002) J Lumin 97:190
6. Gusowski MA, Dominiak-Dzik G, Solarz P, Lisiecki R, Ryba-Romanowski W (2007) J Alloy Compd 438:72
7. Seeber W, Downing EA, Hesselink L, Fejer MM, Ehrt D (1995) J Non-Crystall Solid 189:218
8. Strek W, Legendziewicz J, Lukowiak E, Maruszewski K, Sokolnicki J, Boiko AA, Borzechowska M (1998) Spectrochim Acta A 54:2215
9. Annapurna K, Chakrabarti R, Buddhudu S (2007) J Mater Sci 42:6755. doi:10.1007/s10853-006-1465-x
10. Mazurak Z, Pisarski WA, Gabrys-Pisarska J, Zelechower M (2003) Phys Stat Sol (b) 237(2):581

11. Del Longo L, Ferrari M, Zanghellini E, Bettinelli M, Capobianco JA, Montagna M, Rossi F (1998) J Non-Crystall Solid 231:178
12. Ravi Kumar A, Veeraiah N, Appa Rao B (1997) J Lumin 75:57
13. X-jun Wang, Huang SH, Reeves R, Wells W, Dejneka MJ, Meltzer RA, Yen WM (2001) J Lumin 94–95:229
14. De G, Licciulli A, Nacucchi M (1996) J Non-Crystall Solid 201:153
15. Boiko AA, Poddenezhny EN, Lukowiak E, Strek W, Sokolnicki J, Legendziewicz J (1995) J Appl Spectrosc 62(4):656
16. Biswas A, Chakrabarti S, Acharya HN (1997) Mater Sci Eng B49:191
17. Diallo PT, Boutinaud P, Mahiou R, Coussens JC (1997) Phys Stat Sol (a) 160:255
18. Duan CY, Chen J, Deng SZ, Xu NS, Zhang JH, Liang HB, Su Q (2007) J Vac Sci Technol B25(2):618
19. Swart HC, Greeff AP (2004) Surf Interface Anal 36:1178
20. Psuja P, Hreniak D, Strek WJ (2007) J Nanomater, Article No. 81350. doi:10.1155/2007/81350
21. Ntwaeaborwa OM, Swart HC, Kroon RE, Holloway PH, Botha JR (2006) J Chem Phys Solid 67:1749
22. Ntwaeaborwa OM, Hillie KT, Swart HC (2004) Phys Stat Sol (c) 1(9):2366
23. Kamat PV, Patrick B (1992) J Phys Chem 96:6829
24. Van Dijken A, Makkinje J, Meijerink A (2001) J Lumin 92:323
25. Ntwaeaborwa OM, Holloway PH (2005) Nanotechnology 16:865
26. Biswas A, Acharya HN (1997) Mater Res Bull 32(11):1551
27. de Mello Donega C, Meijerink A, Blasse G (1995) J Appl Spectrosc 62(4):664
28. Isasi-Marin J, Perez-Estebanez M, Diaz-Guera C, Castillo JF, Correcher V, Cuervo-Rodriguez MR (2009) J Phys D-Appl Phys 42(7), Article No. 075418. doi:10.1088/0022-3727/42/7/075418
29. Bang J, Yang H, Holloway PH (2005) J Chem Phys 123:084709. doi:10.1063/1.2007647
30. Swart HC, Oosthuizen L, Holloway PH, Berning GLP (1998) Surf Interface Anal 26:337
31. Swart HC, Hillie KT, Greeff AP (2001) Surf Interface Anal 32:110
32. Thomas S (1974) J Appl Phys 45(1):161
33. Dhlamini MS, Terblans JJ, Ntwaeaborwa OM, Swart HC (2007) Surface Rev Lett 14(4):697